NUKLEONIKA 2018;63(4):95–103
doi: 10.2478/nuka-2018-0012

ORIGINAL PAPER

Modelling the effects of lung cancer motion due to respiration

Marta Adamczyk,
Sebastian Adamczyk,
Tomasz Piotrowski

Abstract. *Background and objectives*: To justify the concept of validating conformal versus intensity-modulated approach in the treatment of non-small cell lung cancer (NSCLC). *Materials and methods*: For 10 patients representative of the spectrum of tumour sizes and locations, two plans were prepared: one with three-dimensional conformal radiation therapy (3DCRT) technique and the other with intensity-modulated radiation therapy (IMRT) technique. Preliminary measurements were performed in static conditions. For each of the field angles considered, the motion kernel was generated to simulate tumour motion trajectories, with the largest amplitude in the cranio-caudal direction of 4, 6, and 8 mm. The measurement results determined the agreement between the planned and measured doses. *Results*: No statistically significant differences were found between the motion patterns, with the smallest amplitudes for clinical target volume in 3DCRT. For IMRT, the significant differences between 0 mm vs. 6 mm and 0 mm vs. 8 mm amplitudes were found. The motion impact on delivered vs. planned doses had less effect on the oesophagus in 3DCRT compared to that in IMRT. The observed differences were comparable for the heart. *Interpretation and conclusions*: For maximal amplitudes below 4 mm, the disagreement between planned and delivered doses can be neglected. However, the amplitudes above 5 mm and 7 mm lead to significant changes in IMRT and 3DCRT dose distribution, respectively.

Keywords: dosimetric plan verification • external beam radiation therapy • lung cancer • respiratory motion

Introduction

Over the past years, a rapid improvement of imaging and radiotherapy treatment techniques has led to a significant increase in therapeutic strategies. Consequently, the quality of a treatment process is evaluated by precision of doses delivered to tumour (target volume) and organs at risk, and a lot of attention is paid to validate the physical aspects of radiation therapy (RT) in each irradiated volume e.g. for patients with tumours affected by respiratory motion. Along with these developments, the optimal use of available techniques still poses a challenge to the irradiation of non-small cell lung cancer (NSCLC) patients [1–3]. Of course, the most important concern is the intra-fraction motion due to breathing. This problem can negate the potential gain of intensity-modulated radiotherapy (IMRT), as motion could distort the shape of an object, both the target and any organ at risk (OAR). More precisely, the use of all the temporally modulated techniques is associated with the risk of the so-called interplay effect. It is named so due to the interplay of tumour motion during the respiratory cycle and the movement of the multileaf collimator (MLC) [4, 5]. The results of the study of Bortfeld *et al*. [6] underlined that due to fluence complexity, in motion conditions,

M. Adamczyk✉, S. Adamczyk#
Medical Physics Department
Greater Poland Cancer Centre
15 Garbary St., 61-866 Poznan, Poland
E-mail: marta.adamczyk@wco.pl
#IntraOp Medical, 570 Del Rey Ave,
94085 Sunnyvale, CA, USA (current affiliation)

T. Piotrowski
Medical Physics Department
Greater Poland Cancer Centre
15 Garbary St., 61-866 Poznan, Poland
and Department of Electroradiology,
University of Medical Sciences,
15 Garbary St., 61-866 Poznan, Poland

Received: 2 July 2018
Accepted: 27 October 2018

severe local overdosages or underdosages would occur. Quantitatively, the effect may result in differences in hot and cold spots by a factor of more than 4 from planned to delivered fluences [7].

Apart from interplay, planned dose distribution may not match the actual one due to dose blurring [4]. The effect is limited to this part of the irradiation field where dose gradient occurs, and thus, its impact can be predicted as the weighted average calculated for two paths of dose distribution, with and without breathing motion [8–10]. As a typical spatial effect, dose blurring is independent of the delivery technique [5, 8]. During all temporary modulated treatment delivery, blurring is strongly associated with interplay between MLC and target movement. For conventional conformal plan, in contrast to the field centre, where the dose gradient is small, on the edge of the field, the effect becomes a serious problem [1, 8]. Consequently, for the three-dimensional conformal radiation therapy (3DCRT) technique, the increase in the safety margin added to the clinical target volume (CTV) is a common method used to compensate the blurring effect. Unfortunately, when a large volume of healthy tissues around the target is irradiated, it leads to increased risk of pulmonary complications [11–14]. As a result of this problem, the authors of the American Association of Physicists in Medicine (AAPM) in Report 91: 'The management of respiratory motion in radiation oncology' suggested that IMRT could conform the spatial dose distribution deposited in a patient more effectively due to the presence of many important organs at risk in this region [8].

As different irradiation schemes are used in particular centres with their in-house opportunities and limitations, the external beam radiation treatment should be applied according to the available technical possibilities of radiation delivery (e.g. the type of immobilization devices or respiratory motion technique used) [15]. In our centre, to justify the concept of validating conformal vs. intensity-modulated approach, a group of patients was chosen representative for the spectrum of tumour sizes and locations. The goal of the retrospective dose distribution simulations was to form a global idea of the quality of IMRT realization by its comparison to 3DCRT dose delivery for patients with tumours affected by respiratory motion. The insight into the difference between the actual and calculated dose distributions for both tumour and OARs was also provided, giving the answer for the question of how big a tumour movement can be compensated while using the standard 1-cm CTV-to-planning target volume (PTV) margin without any motion-compensation strategy.

Material and methods

Patient group

To test the influence of the respiratory motions on the dose distribution agreement, a retrospective group of 10 consecutive patients with NSCLC who were treated in 2012 in our hospital was chosen. The computed tomography (CT) slices acquired at free breathing conditions (patients were guided to breath normally and lightly [3, 16]; the same breathing and couching was repeated before each treatment fraction) were transferred to Eclipse v.10.0 Treatment Planning System (Varian Medical Systems, Palo Alto, CA, USA), where target and OARs were contoured. The CTV included gross tumour volume (GTV) and the region of subclinical malignant disease. Then, CTV was expanded by a uniform 1-cm margin to generate the PTV [17]. The PTV was created to include margins for intra-fraction motion (i.e. breathing) and inter-fraction motion (i.e. setup) [7]. The range of the treated volumes for CTV was from 8.2 cc to 421.8 cc (average: 99.98 cc) and that for PTV was from 53.8 cc to 825.2 cc (average: 247.64 cc). The OARs outlined included the heart, oesophagus, spinal cord, whole lungs (without PTV extraction from lung tissues), and contralateral lung.

External beam treatent planning

For each patient, two plans were prepared using coplanar 3DCRT and IMRT techniques with the elimination of field entrances through the contralateral lung. The 3DCRT plans were realized clinically, while the IMRT plans were simulated for the needs of this study. Both plans were prepared for Clinac 2300C/D (Varian Medical Systems, Palo Alto, CA, USA) and calculated using 6 MV photons delivered in 2 Gy fraction dose to the cumulative dose of 64 Gy [12, 18, 19] with gantry angles and collimator rotations adopted individually (based on patients' anatomy) to obtain optimal sparing of OARs and PTV coverage. The linear accelerator used in the study (Clinac 2300C/D) was equipped with Millennium 120 MLC. The width of the central 40 leaf pairs was 0.5 cm. The 3DCRT plan geometry consisted of three fields. To achieve enhanced dose homogeneity within the treated volume with the elimination of hot and cold spots (which makes the resulting dose distribution sensitive to possible misalignment errors), field weighting and wedges were used. In the next step, for patients included in this study and treated by 3DCRT, we prepared simulation of a five-field sliding window IMRT plan. The dose calculation was provided with the inverse planning algorithm available in the Eclipse Helios module. The final dose distributions for clinically realized 3DCRT and simulated IMRT plans were computed with dose corrected for heterogeneities using analytical anisotropic algorithm (AAA) with a spatial resolution of 0.25 cm [13]. For both techniques, PTV dose inhomogeneity varied between –5% and +7%. When it was not possible to fulfil these criteria, 99% of the PTV had to receive 95% of the prescribed dose. Hot spots with doses higher than 107% were accepted only if they were in less than 1% of the PTV volume. For both plans, the same PTV to CTV margin was used. Doses delivered to OARs were evaluated according to the dose-volume criteria specified in our hospital protocol for lung cancer treatment that correlate with the

recommendations presented by Marks *et al*. [20]. During the forward (3DCRT) or inverse (IMRT) optimization process, we tried to obtain acceptable doses in OARs. The specified dose constraints were the following: (1) lungs – mean dose lower than 16 Gy; the volume receiving >20 Gy limited to <37%, and volume receiving >5 Gy limited to <70%; the doses in contralateral lung were minimalized as low as possible; (2) heart – mean dose lower than 26 Gy; the volume receiving >45 Gy limited to <50%; (3) oesophagus – mean dose lower than 34 Gy; the volume receiving >50 Gy limited to <40%, the volume receiving >55 Gy limited to <33% and the volume receiving >60 Gy limited to <16 cc, and (4) spinal cord – maximum dose lower than 48 Gy. The dose constraints in OARs used in the optimization process during plan preparation were not differentiated due to respiratory amplitude. Figure 1 shows a dosimetric comparison of IMRT and 3DCRT plans for a randomly selected patient included in the study: (a) cumulative dose-volume histogram for PTV and OARs and for two techniques of irradiation (IMRT and 3DCRT), (b) transversal slice of the dose distribution for IMRT and (c) transversal slice of the dose distribution for 3DCRT.

Respiratory motion modelling

For each of the field angles considered, the motion kernel (three-dimensional motion of the target relative to the treatment couch), characterized by 4-s breathing period, was generated [4, 21–24]. It was defined as the projection of the tumour motion perpendicular to the beam's eye view (BEV), as motors of the used robotic platform (MotionSimXY/4D; Sun Nuclear, Melbourne, FL, USA) drive its tabletop in the two spatial dimensions orthogonal to the beam central axis [4, 21, 22]. The motion kernels used, derived from the literature data [23], led to simulate three tumour motion trajectories, with the largest movement amplitude in the cranio-caudal direction of 4, 6 and 8 mm. Additionally, the sets of reference measurements were made in static conditions (0 mm amplitude). The dose distributions were measured using a 2D array of 1527 diodes with a size of 0.019 cc and a resolution (distance between two detectors) equal to 0.75 cm (MapCHECK 2; Sun Nuclear, Melbourne, FL, USA) attached to the tabletop of the robotic platform and positioned at 100 cm source-to-axis distance (SAD) with 3 cm of solid water (water

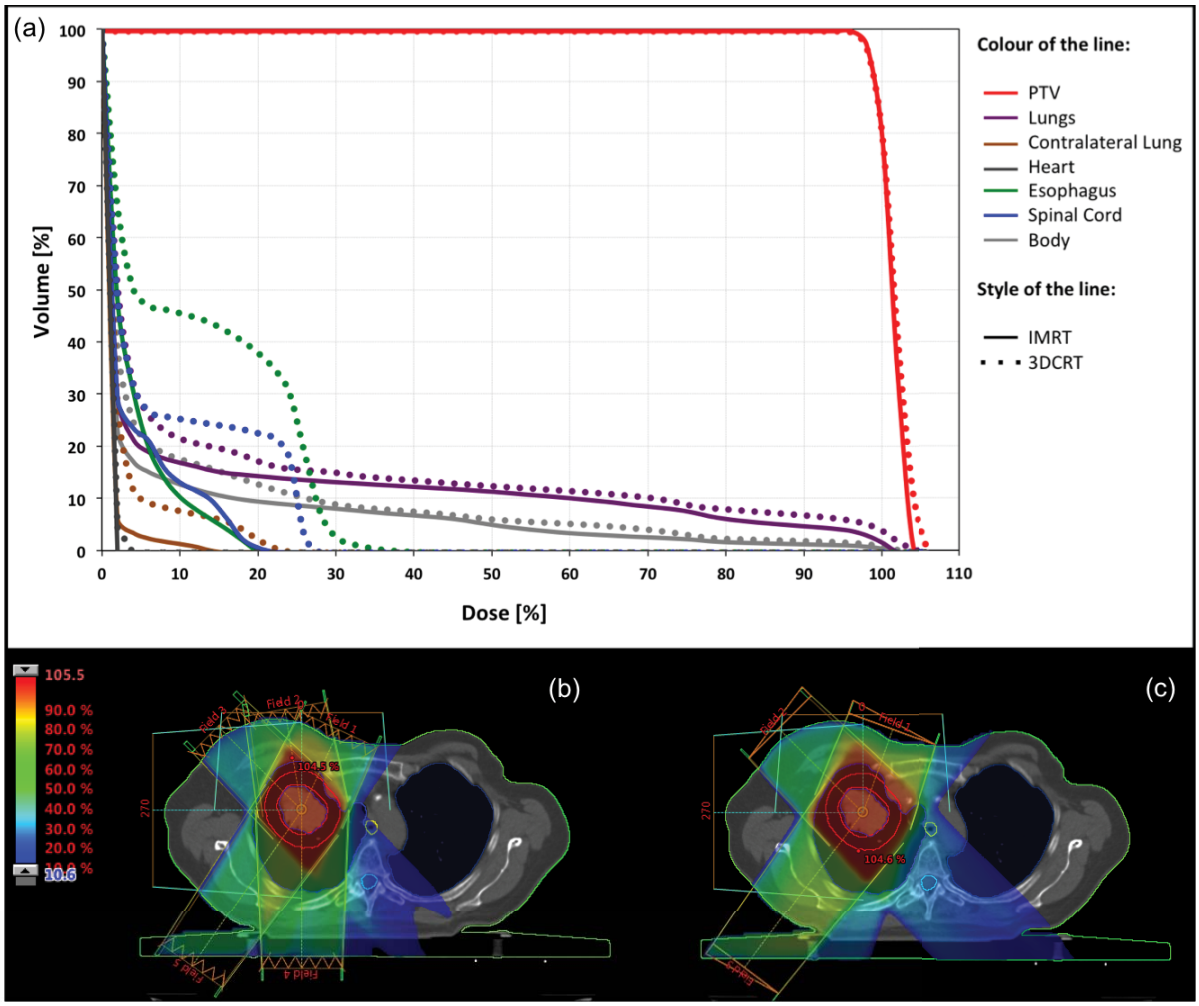

Fig. 1. A dosimetric comparison of IMRT and 3DCRT plans for randomly selected patient: (a) cumulative dose volume histogram for PTV (red), lungs (purple), contralateral lung (orange), heart (dark grey), oesophagus (green), spinal cord (blue) and whole body of the patient (light grey) and for two techniques of irradiation (IMRT – solid line and 3DCRT – dotted line); (b) transversal slice of the dose distribution for IMRT and (c) transversal slice of the dose distribution for 3DCRT.

Fig. 2. The robotic platform (MotionSimXY/4D; Sun Nuclear, Melbourne, FL, USA) with diode array (MapCHECK 2; Sun Nuclear, Melbourne, FL, USA) and water equivalent built-up (3 cm of solid water).

equivalent build-up) placed on the top of the array [4, 21] as presented in Fig. 2.

The single beam from each treatment plan was recalculated in the treatment planning system by copying the dose distribution (field size, MLC and monitor units (MUs), were preserved) from patient to the CT of the used measurement set. Thus, all measurements were performed from 0° gantry angle based on the assumption that the patients' breathing pattern was regular and reproducible; however, the initial respiratory phase was defined as a random parameter [4, 7, 21]. The relative dose to detector was calculated by multiplying the relative correction factor for detector by the result of the equation, which took into account the initial and final voltages for the detector, the voltage drift (background, measured prior to measurement) and time between measurement's start and stop. The obtained relative dose values were saved in a certain data file. The comparison between statically planned dose distribution (RT plan and RT dose files exported from the treatment planning system) and measured one (delivered with breathing motion simulation) was performed using SNC Patient software (Sun Nuclear, Melbourne, FL, USA). Precisely, the difference in the position of points with the same values of measured and calculated doses was assessed based on the gamma index (γ) analysis [25] with 3-mm criteria of distance to agreement (DTA) and dose difference (ΔD) of 3%. Thus, $\gamma \leq 1$ and $\gamma > 1$ indicate the agreement and disagreement between these two doses, respectively, with 3% dose difference within 3-mm distance between analysed doses as the cut-off criterion. After analysing the γ values for each dose points, the average γ was calculated. The first criterion to assess the plan as valid for treatment was that the average γ was <0.6. Then, to be sure that in most of the points, the measured dose value was correct, the score was evaluated by defining the percent value of the measured points, for which γ parameter was correct. The score value, which can be assumed as positive verification result (>95%), was the second plan evaluation criterion.

Apart from the agreement of the whole delivered field, the evaluation was separately performed both for the target and OARs. Structures presented in each BEV were analysed, taking into account the total number of array's detectors within the given structures. In this part of the analysis, the additional option for characterizing the tolerance criterion was used, aiming to calculate the number of detectors activated within the analysed structure. The number of measuring points, which did not meet the imposed criteria, was analysed by dividing them into two groups. The parameters, which described the number of detectors that measured lower dose compared to reference dose from the treatment plan, were named failed cold points. In contrast, the number of failed hot points indicated the number of measuring points that traced the higher dose.

Finally, the analysis was performed based on 320 dose distributions obtained for each field under the experimental conditions, giving 32 dose distributions per patient to compare. Nine dose distributions obtained per patient were used to evaluate the differences detected among three-field 3DCRT techniques due to simulated breathing. Other 15 dose distributions were examined to investigate how motion affected the five-field IMRT delivery. The remaining eight (three for 3DCRT and five for IMRT) dose distributions were acquired to check the agreement between the reference and obtained measurements in static conditions (0 mm). The results of agreement for 0 mm amplitude were set as reference for the rest of comparisons where non-zero amplitude of motion was used.

To compare the parameters, which described the quality of plan delivery in different breathing conditions, non-parametric Friedman ANOVA was performed. If the determined P value was ≤ 0.05, the post-hoc analysis (two-tailed Nemenyi test) was used to verify which group was responsible for the difference.

Results

According to the prepared plans, IMRT showed trends to better spare the doses delivered to the lungs (Table 1).

Based on Friedman test, statistically significant CTV dose degradation in motion conditions was found. The post-hoc analysis revealed that taking into account the CTV score parameter in 3DCRT, the difference was found for the 8 mm amplitude when it was compared with 0 mm amplitude. In the case of IMRT, for all analysed parameters such as score, failed cold and failed hot, the significant differences between 0 mm vs. 6 mm and 0 mm vs. 8 mm were found on the basis of post-hoc analysis. All the differences detected among CTV resulted from the disagreement related to obtaining lower doses than calculated in 3DCRT and IMRT plans (failed cold). Additionally, for IMRT plans, overdose was detected in selected points of CTV (failed hot).

After adding the components associated with the respiratory movement to the lung dose analysis, the only 3DCRT parameter that did not reach a statistical significance was the number of contralateral lung failed hot points ($P > 0.05$ comparing all simulated movements and static conditions). The corresponding value of this parameter in the IMRT plans showed significance, which, according

Table 1. Descriptive statistical comparison of doses received by OARs in 3DCRT and IMRT plans

Organ at risk	Dose parameter	Statistical parameter	Treatment technique	
			3DCRT	IMRT
Lungs	V_{5Gy} [%]	Mean	35.81	32.27
		Min-Max	21.63–72.83	18.12–78.32
		SD	16.35	17.61
	V_{10Gy} [%]	Mean	28.74	23.59
		Min-Max	18.64–60.43	13.92–57.42
		SD	12.84	12.66
	V_{15Gy} [%]	Mean	22.47	18.36
		Min-Max	14.64–53.11	10.13–38.92
		SD	11.40	8.24
Contralateral lung	V_{5Gy} [%]	Mean	18.71	18.13
		Min-Max	0.00–61.70	0.07–78.21
		SD	20.71	23.42
	V_{10Gy} [%]	Mean	12.30	8.40
		Min-Max	0.00–50.55	0.00–48.50
		SD	17.10	15.25
	V_{15Gy} [%]	Mean	6.34	3.49
		Min-Max	0.00–41.84	0.00–21.54
		SD	13.28	6.82
Oesophagus	D_{mean} [Gy]	Mean	8.63	6.90
		Min-Max	0.60–27.60	1.60–26.40
		SD	9.75	9.66
Heart	$D_{50\%}$ [Gy]	Mean	4.48	2.92
		Min-Max	0.20–15.80	0.10–15.00
		SD	5.02	4.83

A set of standard physical quantities were described as Min-Max (the range between minimum and maximum values). Mean – mean value. SD – standard deviation. V_{YGy} – volume receiving at least Y [Gy]. D_{max} – the maximum dose received by the analysed organ. D_{mean} – the mean dose received by the analysed organ. $D_{50\%}$ – dose received by 50% of the analysed organ.

to the post-hoc analysis, was found for the 0 mm vs. 8 mm amplitude. Other IMRT statistics prepared for contralateral lung and both lungs together revealed considerable differences between the 0 mm vs. 6 mm and 0 mm vs. 8 mm amplitudes (P values' details are given in Table 2).

Similar results were obtained for 3DCRT lung analysis, but without post-hoc statistical significance between the 0 mm vs. 6 mm amplitude for both lungs' score and failed hot points in both lungs.

Among all analysed IMRT parameters for OARs, the only lack of statistical significance was found for failed hot points (Friedman ANOVA $P = 0.061$) in the oesophagus, whereas for the score and failed cold points, the difference was found for the 0 mm vs. 8 mm amplitude. No matter which parameter was tested for the oesophagus in the 3DCRT, the difference between the static and any simulated motion condition was insignificant ($P > 0.050$). The lack of significance was also detected for failed hot points (Friedman ANOVA $P = 0.051$) in the heart using 3DCRT. The number of failed cold points and the score for the heart changed significantly for 0 mm vs. 8 mm amplitude for 3DCRT. When IMRT technique was used, for all parameters analysed in the heart, the differences were found between the 6 mm and 8 mm motion amplitudes as compared to amplitudes in the static situation. The information about statistically significant differences between simulated breathing motion amplitudes among CTV and OARs is summarized in Table 2.

The average score and average γ found after analysing the agreement between the planned and measured 3DCRT distribution in no motion conditions equalled 99.10% and 0.247, respectively. Subsequent measurements for the 4-mm amplitude decreased the average score value to 98.10%. For higher simulated motion amplitudes, the average score equalled 97.08% (for 6 mm) and 93.86% (for 8 mm). The average γ increased from 0.247 (for 0 mm) through 0.262 (for 4 mm) and 0.279 (for 6 mm) reaching 0.302 (for 8 mm).

For IMRT, the average score (mean value for 50 fields) for the static target equalled 99.43% and the average γ equalled 0.330. When the breathing trajectory with the amplitude of 4 mm was applied, we found the average score of 97.81% and the average γ value of 0.386, which fitted well with the plan acceptance criteria. For the 6 mm amplitude, the average score was 94.18% and average γ value was 0.468. However, when the 8 mm amplitude was applied, we observed a significant change in analysed parameters: average score and γ value of 83.68% and 0.572, respectively.

The averaged results of the score for each of 3DCRT and IMRT fields are presented in Figs. 3 and 4.

Discussion

In this study, two different techniques were verified for the respiratory motion effect on actually deliv-

Table 2. Statistically significant differences revealed between different breathing motion amplitudes for score, failed cold and failed hot points among CTV and OARs

Structure	Parameter	Significant differences for each technique (with P values)	
		3DCRT	IMRT
CTV	Score	0 mm vs. 8 mm ($P = 0.001$)	0 mm vs. 6 mm ($P = 0.003$) 0 mm vs. 8 mm ($P < 0.001$)
	Failed cold	0 mm vs. 8 mm ($P = 0.001$)	0 mm vs. 6 mm ($P = 0.002$) 0 mm vs. 8 mm ($P < 0.001$)
	Failed hot	None	0 mm vs. 6 mm ($P = 0.017$) 0 mm vs. 8 mm ($P < 0.001$)
Lungs	Score	0 mm vs. 8 mm ($P = 0.000$)	0 mm vs. 6 mm ($P = 0.006$) 0 mm vs. 8 mm ($P < 0.001$)
	Failed cold	0 mm vs. 6 mm ($P = 0.014$) 0 mm vs. 8 mm ($P < 0.001$)	0 mm vs. 6 mm ($P = 0.004$) 0 mm vs. 8 mm ($P < 0.001$)
	Failed hot	0 mm vs. 8 mm ($P = 0.001$)	0 mm vs. 6 mm ($P = 0.037$) 0 mm vs. 8 mm ($P < 0.001$)
Contralateral lung	Score	0 mm vs. 8 mm ($P = 0.002$)	0 mm vs. 6 mm ($P = 0.013$) 0 mm vs. 8 mm ($P < 0.001$)
	Failed cold	0 mm vs. 6 mm ($P = 0.040$) 0 mm vs. 8 mm ($P = 0.001$)	0 mm vs. 6 mm ($P = 0.007$) 0 mm vs. 8 mm ($P < 0.001$)
	Failed hot	None	0 mm vs. 8 mm ($P = 0.000$)
Oesophagus	Score	None	0 mm vs. 8 mm ($P = 0.004$)
	Failed cold	None	0 mm vs. 8 mm ($P = 0.049$)
	Failed hot	None	None
Heart	Score	0 mm vs. 8 mm ($P = 0.018$)	0 mm vs. 6 mm ($P = 0.019$) 0 mm vs. 8 mm ($P = 0.003$)
	Failed cold	0 mm vs. 8 mm ($P = 0.040$)	0 mm vs. 6 mm ($P = 0.019$) 0 mm vs. 8 mm ($P = 0.005$)
	Failed hot	None	0 mm vs. 8 mm ($P = 0.014$)

ered dose distribution. Consequently, this paper addresses an important issue, which is the effect of tumour motion on dose distributions for external photon therapy. Like in clinical situation, both the effects of patient motion and machine dynamics were integrated in the results. To provide meaningful clinical insight, the analysis results were carried out carefully and thoughtfully field by field. The concept of the field-by-field analysis resulted from the technical solutions (MotionSimXY/4D integrated with the MapCHECK 2) that are available in the centre where the study was preformed. It should be noted that there is possibility to 'plan-based' analysis that could be realized by software solution implemented in 3DVH software (Sun Nuclear, Melbourne, FL, USA). Unfortunately, during the realization of this study, 'plan-based' analysis was not possible for us.

The authors are aware that the gamma-index method is a mathematical rather than a clinical concept, and one can argue that what is statistically significant may not be significant clinically. However,

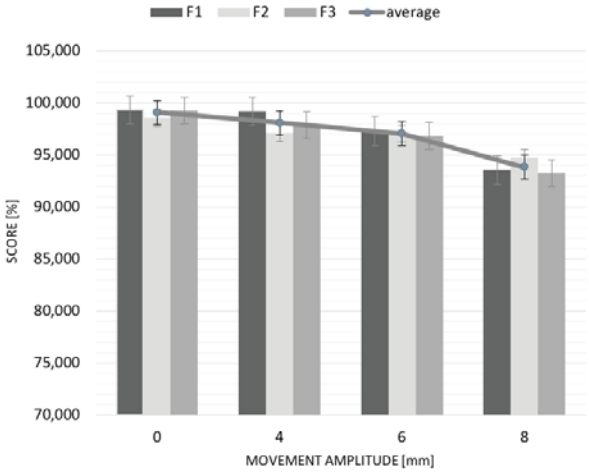

Fig. 3. Average score results for similar gantry angles (fields F1-F3) of 3DCRT plans. Error bars for each field were presented in grey. Error bars averaged over the three fields for each movement amplitude was presented in black.

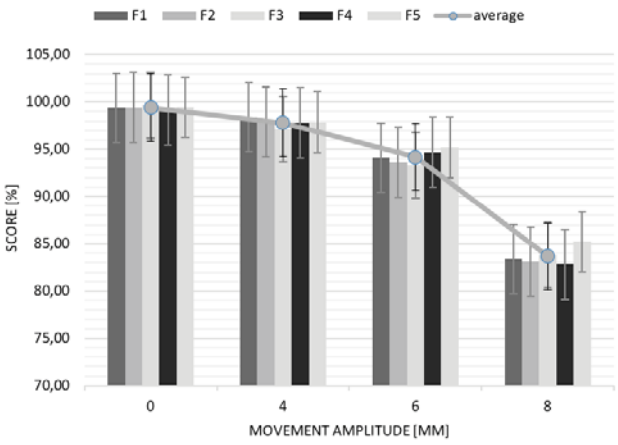

Fig. 4. Average score results for similar gantry angles (fields F1-F5) of IMRT plans. Error bars for each field were presented in grey. Error bars averaged over the five fields for each movement amplitude was presented in black.

to perform fair analysis, such a mathematical concept, well-understood and widely used around the world, is needed as a verification tool. This allowed us to achieve the clear and useful answer about respiratory motion impact on delivered doses. Owing to the lack of such literature findings, the obtained results are very important for many physicians and physicists in countless, smaller cancer centres that do not have any sophisticated motion compensation technology (e.g. 4DCT, gating or tracking) at their disposal.

During both 3DCRT and IMRT planning, the avoidance of contralateral lung was preferred. It has a higher priority than the plan conformity. That is why, although it is rather intuitive that IMRT involves more fields and, consequently, larger volume of surrounding tissues are exposed to lower doses, our treatment planning comparison did not show this tendency. Even not for the most complex plans, taking into account the doses delivered to other OARs, our comparison of 3DCRT and IMRT results confirms that dose decrease in OARs is possible with IMRT. This illustrates that even when the unfavourable 'flat' plan geometry is chosen, the higher dose gradients are achieved with IMRT.

The presented results achieved for CTV confirmed the literature findings that 3DCRT, compared to IMRT, is less affected by respiratory movement [26]. The larger the respiratory motion and IMRT modulation, the higher the observed differences [21, 27]. Thus, when considering to implement IMRT and eliminate the interplay effect to a clinically acceptable level, single-fraction delivery time should be taken into account. Owing to single-fraction delivery time lengthening, the initial respiratory phase would have less effect on the dose delivered to CTV [21, 28]. Analysing a problem from another perspective, the decrease in dose variation is associated with the decrease in dose rate [29, 30]. Our plans were generated with the dose rate of 300 MU/min, which is more than twice as low as the one used in modern machines like TomoTherapy or CyberKnife.

According to most literature reports, the cranio-caudal respiratory movement is predominant for the majority of patients [23, 31]. Some authors have tried to find the correlation between breathing motion and tumour location. In this way, Erridge *et al*. [32] or Gendrin *et al*. [23] reported the largest motion (for individual patient even up to 33.5 mm) for tumours in the lower lobes, due to their location near the diaphragm. In contrast, the target detected in the apex of the lung is characterized by strongly reduced motion [23]. For mediastinal tumours, the breathing impact may be more complicated to predict due to the heartbeat effect, detected when PTV encompasses the heart wall [8, 23, 33]. Another aspect of breathing impact should be linked to the possible dependence between tumour size and its motion. The results achieved in our study group showed that the worst agreement between planned and delivered doses was achieved for smaller tumours. This problem of the part of tumour volume escaping from the beam as a result of its breathing explains the interplay effect and, thus, is of importance especially for IMRT delivery. Therefore, precise breathing and dosimetric verification are of utmost importance to ensure correct planning and delivery for lung cancer treatment by eliminating the deviation between the intended and delivered dose distributions.

It should be noted that for all analyses in this study, the resolution used for the calculations of the doses differs from the resolution of measurements (0.25 cm vs. 0.75 cm). Resulting from this fact, uncertainty that burdens the comparisons of the calculations with the measurements is a component of differences that are visible during average score analysis for static conditions (0 mm amplitude), for both techniques (3DCRT – average score 99.1% and IMRT – average score 99.43%). This uncertainty is stable for comparisons between reference condition (static, 0 mm amplitude) and other conditions that take into account amplitudes of movements (e.g. 4, 6 and 8 mm).

Conclusions

Searching for the balance between probability of cure and complications, the performed 3DCRT and IMRT validation proves the potential for effective and patient-friendly delivery. The truth is that the 3DCRT is safe in a greater range of respiratory movement amplitudes. On the other hand, the study results showed that the IMRT application affords possibilities for further optimizing the therapeutic ratio for selected patients. Of course, IMRT could cause the tumour underdosage due to the interplay effect. It is therefore important to verify the amplitude of individual patient breathing motion trajectory. For maximal amplitudes below 4 mm, the disagreement between planned and delivered doses can be neglected. However, an amplitude above 5 mm leads to significant changes in delivered dose distribution. In contrast, during 3DCRT treatment realization, for maximal amplitudes above 7 mm, a significant disagreement was found between the planned and delivered doses.

Conflict of interest statement. Conflicts of interest: none.

Acknowledgment. This work was supported by the Greater Poland Cancer Centre, Poznan, Poland (grant no. 21/2014(80) dated 22.08.2014).

References

1. Lambin, P., Petit, S. F., Aerts, H. J. W. L., van Elmpt, W. J. C., Oberije, C. J. G., Starmans, M. H. W., van Stiphout, R. G. P. M., van Dongen, G. A. M. S., Muylle, K., Flamen, P., Dekker, A. L. A. J., & De Ruysscher, D. (2010). The ESTRO Breur Lecture 2009. From population to voxel-based radiotherapy: Exploiting intra-tumour and intra-organ heterogeneity for advanced treatment of non-small cell lung cancer.

Radiother. Oncol., *96*, 145–152. DOI: 10.1016/j.radonc.2010.07.001.
2. Isa, N. (2014). Evidence based radiation oncology with existing technology. *Rep. Pract. Oncol. Radiother.*, *19*, 259–266. DOI: 10.1016/j.rpor.2013.09.002.
3. Pan, T., Lee, T. Y., Rietzel, E., & Chen, G. T. (2004). 4D-CT imaging of a volume influenced by respiratory motion on multi-slice CT. *Med. Phys.*, *31*, 333–3340. DOI: 10.1118/1.1639993.
4. Ehler, E. D., & Tomé, W. A. (2009). Step and shoot IMRT to mobile targets and techniques to mitigate the interplay effect. *Phys. Med. Biol.*, *54*, 4311–4324. DOI: 10.1088/0031-9155/54/13/023.
5. Nelms, B. E., Opp, D., Zhang, G., Moros, E., & Feygelman, V. (2014). Motion as perturbation. II. Development of the method for dosimetric analysis of motion effects with fixed-gantry IMRT. *Med. Phys.*, *41*, 061704. DOI: 10.1118/1.4873691.
6. Bortfeld, T., Jokivarsi, K., Goitein, M., Kung, J., & Jiang, S. B. (2002). Effects of intra-fraction motion on IMRT dose delivery: statistical analysis and simulation. *Phys. Med. Biol.*, *47*, 2203–2220. DOI: http://dx.doi.org/10.1088/0031-9155/47/13/302.
7. Sterpin, E., Janssens, G., de Xivry, J. O., Goossens, S., Wanet, M., Lee, J. A., Delor, A., Bol, V., Vynckier, S., Gregoire, V., & Geets, X. (2012). Helical tomotherapy for SIB and hypo-fractionated treatments in lung carcinomas: A 4D Monte Carlo treatment planning study. *Radiother. Oncol.*, *104*, 173–180. DOI: 10.1016/j.radonc.2012.06.005.
8. Keall, P. J., Mageras, G. S., Balter, M. J., Emery, R. S., Forster, K. M., Jiang, S. B., Kapatoes, J. M., Low, D. A., Murphy, M., Murray, B. R., Ramsey, C. R., van Herk, M., Vedam, S. S., Wong, J. W., & Yorke, E. (2006). The management of respiratory motion in radiation oncology report of AAPM Task Group 76. *Med. Phys.*, *33*, 3874–3900. DOI: 10.1118/1.2349696.
9. Tudor, G. S. J., Harden, S. V., & Thomas, S. J. (2014). Three-dimensional analysis of the respiratory interplay effect in helical tomotherapy: Baseline variations cause the greater part of dose inhomogeneities seen. *Med. Phys.*, *41*, 031704. DOI: 10.1118/1.4864241.
10. Adamczyk, M., & Piotrowski, T. (2017). Respiratory motion and its compensation possibilities in the modern external beam radiotherapy of lung cancer. *Nowotwory J. Oncol.*, *67*, 292–296. DOI: 10.5603/NJO.2017.0048.
11. Ehrhardt, J., Werner, R., Säring, D., Frenzel, T., Lu, W., Low, D., & Handels, H. (2007). An optical flow based method for improved reconstruction of 4D CT data sets acquired during free breathing. *Med. Phys.*, *34*, 711–721. DOI: 10.1118/1.2431245.
12. Bai, L., Zhao, J., Yu, H., Zhao, N., Liu, D., Zhong, W., & Zhao, Y. (2013). The CD36 dynamic change after radiation therapy in lung cancer patients and its correlation with symptomatic radiation pneumonitis. *Radiother. Oncol.*, *107*, 389–391. DOI: 10.1016/j.radonc.2013.04.014.
13. Farr, K. P., Khalil, A. A., Knap, M. M., Møller, D. S., & Grau, C. (2013). Development of radiation pneumopathy and generalised radiological changes after radiotherapy are independent negative prognostic factors for survival in non-small cell lung cancer patients. *Radiother. Oncol.*, *107*, 382–388. DOI: 10.1016/j.radonc.2013.04.024.
14. Piotrowski, T., Matecka-Nowak, M., & Milecki, P. (2005). Prediction of radiation pneumonitis: dose volume histogram analysis in 62 patients with non-small cell lung cancer after three dimensional conformal radiotherapy. *Neoplasma*, *52*, 56–62.
15. Maciejczyk, A., Skrzypczyńska, I., & Janiszewska, M. (2014). Lung cancer. Radiotherapy in lung cancer: Actual methods and future trends. *Rep. Pract. Oncol. Radiother.*, *19*, 353–360. DOI: 10.1016/j.rpor.2014.04.012.
16. Peguret, N., Dahele, M., Cuijpers, J. P., Slotman, B. J., & Verbakel, W. F. (2013). Frameless high dose rate stereotactic lung radiotherapy: Intrafraction tumor position and delivery time. *Radiother. Oncol.*, *107*, 419–422. DOI: 10.1016/j.radonc.2013.04.019.
17. Kępka, L., Bujko, K., Bujko, M., Matecka-Nowak, M., Sałata, A., Janowski, H., Rogowska, D., Cieślak-Żerańska, E., Komosińska, K., & Zawadzka, A. (2013). Target volume for postoperative radiotherapy in non-small cell lung cancer: results from a prospective trial. *Radiother. Oncol.*, *108*, 61–65. DOI: 10.1016/j.radonc.2013.05.023.
18. Din, O. S., Harden, S. V., Hudson, E., Mohammed, N., Pemberton, L. S., Lester, J. F., Biswas, D., Magee, L. O., Tufail, A., Carruthers, R., Sheikh, G., Gilligan, D., & Hatton, M. Q. F. (2013). Accelerated hypo-fractionated radiotherapy for non small cell lung cancer: Results from 4 UK centres. *Radiother. Oncol.*, *109*, 8–12. DOI: 10.1016/j.radonc.2013.07.014.
19. Filippi, A. R., Franco, P., & Ricardi, U. (2014). Is stereotactic ablative radiotherapy an alternative to surgery in operable stage I non-small cell lung cancer? *Rep. Pract. Oncol. Radiother.*, *19*, 275–279. DOI: 10.1016/j.rpor.2013.05.005.
20. Marks, L. B., Yorke, E. D., Jackson, A., Ten Haken, R. T., Constine, L. S., Eisbruch, A., Bentzen, S. M., Nam, J., & Desay, J. O. (2010). The use of normal tissue complication probability (NTCP) models in the clinic. *Int. J. Radiat. Oncol. Biol. Phys.*, *76*, S10–S19. DOI: 10.1016/j.ijrobp.2009.07.1754.
21. Ehler, E. D., Nelms, B. E., & Tomé, W. A. (2007). On the dose to a moving target while employing different IMRT delivery mechanisms. *Radiother. Oncol.*, *83*, 49–56. DOI: 10.1016/j.radonc.2007.02.007.
22. Adamczyk, S., Piotrowski, T., & Adamczyk, M. (2013). Dose distribution verification in a moving target using moving platform and 2D diode array. *Med. Phys.*, *40*(6,Pt.14), S255. DOI: https://doi.org/10.1118/1.4814658.
23. Gendrin, C., Furtado, H., Weber, C., Bloch, C., Figl, M., Pawiro, S. A., Bergmann, H., Stock, M., Fichtinger, G., Georg, D., & Birkfellner, W. (2012). Monitoring tumor motion by real time 2D/3D registration during radiotherapy. *Radiother. Oncol.*, *102*, 274–280. DOI: 10.1016/j.radonc.2011.07.031.
24. Udrescu, C., Jalade, P., de Bari, B., Michel-Amadry, G., & Chapet, O. (2012). Evaluation of the respiratory prostate motion with four-dimensional computed tomography scan acquisitions using three implanted markers. *Radiother. Oncol.*, *103*, 266–269. DOI: 10.1016/j.radonc.2012.03.016.
25. Low, D. A., Harms, W. B., Mutic, S., & Purdy, J. A. (1998). A technique for the quantitative evaluation of dose distributions. *Med. Phys.*, *25*, 656–661. DOI: 10.1118/1.598248.

26. Cai, J., Malhotra, H. K., & Orton, C. G. (2014). A 3D-conformal technique is better than IMRT or VMAT for lung SBRT. *Med. Phys.*, *41*, 040601. DOI: 10.1118/1.4856175.
27. Chui, C. S., Yorke, E., & Hong, L. (2003). The effects of intra-fraction organ motion on the delivery of intensity-modulated field with a multileaf collimator. *Med. Phys.*, *30*, 1736–1746. DOI: 10.1118/1.1578771.
28. Kang, H., Yorke, E. D., Yang, J., Chui, C. S., Rosenzweig, K. E., & Amols, H. I. (2010). Evaluation of tumor motion effects on dose distribution for hypofractionated intensity-modulated radiotherapy of non-small-cell lung cancer. *J. Appl. Clin. Med. Phys.*, *11*(3), 78–89.
29. Jiang, S. B., Pope, C., Jarrah, K. M., Kung, J. H., Bortfeld, T., & Chen, G. T. (2003). An experimental investigation on intra-fractional organ motion effects in lung IMRT treatments. *Phys. Med. Biol.*, *48*, 1773–1784. DOI: https://dx.doi.org/10.1088/0031-9155/48/12/307.
30. Court, L. E., Wagar, M., Ionascu, D., Berbeco, R., & Chin, L. (2008). Management of the interplay effect when using dynamic MLC sequences to treat moving targets. *Med. Phys.*, *35*(5), 1926–1931. DOI: 10.1118/1.2896083.
31. Ge, Y., O'Brien, R. T., Shieh, C. C., Booth, J. T., & Keall, P. J. (2014). Toward the development of intrafraction tumor deformation tracking using a dynamic multi-leaf collimator. *Med. Phys.*, *41*, 061703. DOI: 10.1118/1.4873682.
32. Erridge, S. C., Seppenwoolde, Y., Muller, S. H., van Herk, M., De Jaeger, K., Belderbos, J. S. A., Boersma, L. J., & Lebesque, J. V. (2003). Portal imaging to assess set-up errors, tumor motion and tumor shrinkage during conformal radiotherapy of non-small cell lung cancer. *Radiother. Oncol.*, *66*, 75–85. DOI: http://dx.doi.org/10.1016/S0167-8140(02)00287-6.
33. White, B. M., Santhanam, A., Thomas, D., Min, Y., Lamb, J. M., Neylon, J., Jani, S., Gaudio, S., Srinivasan, S., Ennis, D., & Low, D. A. (2014). Modeling and incorporating cardiac-induced lung tissue motion in a breathing motion model. *Med. Phys.*, *41*, 043501. DOI: 10.1118/1.4866888.